

SYNTHESIS OF WO₃/TiO₂ (B) NANOWIRES BY HYDROTHERMAL METHOD

K. PAUEKPHONG^a, K. KOOPTARNOND^a, M. KHANGKHAMANO^{a*},
L. SIKONG^a, M. MASAE^b

^a*Department of Mining and Materials Engineering, Faculty of Engineering,
Prince of Songkla University, Hat Yai, 90112 Thailand.*

^b*Department of Industrial Engineering, Faculty of Engineering, Rajamangala
University of Technology Srivijaya, Songkhla, 90000 Thailand*

Monoclinic titanium oxide (TiO₂ (B) phase) nanowires were fabricated using hydrothermal method. To modify electronic properties of the as-synthesized nanowires, WO₃ was doped (WO₃/TiO₂(B)NWs) at various dosages via hydrothermal technique and characterized by XRD, FESEM, EDX, UV-vis and XPS. The effect of dosage on crystallite size, lattice parameters, cell volume, band gap energy, and defect concentration was studied. The findings showed that crystallite size was significantly reduced when the TiO₂(B) nanowires were doped with WO₃. Lattice parameters were altered and cell volume decreased with the increased WO₃ dosage. The highest defect concentration was achieved when 5 mol% doped WO₃ was incorporated, suggesting potential applications in electrical and electronics fields.

(Received June 20, 2019; Accepted December 5, 2019)

Keywords: TiO₂(B) phase, Hydrothermal, WO₃ doped TiO₂, Defect

1. Introduction

Titanium dioxide (TiO₂) is of great practical importance due to its high photoreactivity, nontoxicity, stability, and low cost [1-3]. TiO₂ has three well-known crystallographic forms; tetragonal (anatase and rutile), orthorhombic (brookite) and monoclinic (TiO₂(B)). TiO₂(B) phase (a = 12.16 Å, b = 3.74 Å, c = 6.51 Å, β = 107.29°) is a metastable polymorph formed by the dehydration of layered or open-tunnel structured hydrogen titanate, which was first synthesized in 1980 [4-7]. TiO₂(B) is used in a range of applications including lithium-ion battery [8], solar cells [9, 10] and catalyst [11]. To improve electronic and electrical properties of TiO₂, structure modifications have been advised. These include the fabrication of TiO₂ in the form of zero- and one-dimensional nanostructures, modification of crystal or phase structure, incorporating with metal, non-metal, and/or oxide dopants, as well as hybrid with other nanostructures.

Among the oxide dopants, tungsten oxide (WO₃) is attracted and used as a dopant in this work because it is n-type semiconductor with narrow band gap energy (2.8 eV) and the efficiency of electron-hole pair separation, and the transfer rate of charge carriers in TiO₂ [12, 13]. It has been found that doping WO₃ into TiO₂ crystal structure can improve photocatalytic activities in degradation of organic compounds, including a large fraction of environmental toxins [14-16]. Furthermore, WO₃-doped TiO₂ can be a better visible light absorption than the pure TiO₂. In addition, in general, nanosized semiconductor materials usually contain a large amount of defect concentration. It was suggested that the defect concentration has an important role in photophysical and photochemical process [17, 18]. WO₃-doped TiO₂ significantly enhances photoelectric performance of TiO₂ [18, 19] because of surface and size effects, caused by the increase in the defect concentration on the surfaces of the semiconductor material and hence the enhancement in mobile charge carriers.

To synthesize one-dimensional (1-D) TiO₂(B), i.e. nanowires (NWs) and nanobelts (NBs), a number of methods have been reported [9, 10, 20, 21]. Among them, hydrothermal method has been expanded to prepare other TiO₂-related 1-D nanomaterials, such as potassium titanium oxide

(K₂Ti₆O₁₃) NWs [22], hydrogen trititanate (H₂Ti₃O₇) and hydrogen hexatitanate (H₂Ti₆O₁₃) nanofibers [23], and TiO₂(B) NWs [21]. In general, hydrothermal treatment at a slightly higher temperature than 150 °C or in stronger alkali solution (conc. NaOH(aq.) or KOH(aq.)) results in the formation of solid NWs (or even long nanofibers) rather than scrolled nanotubes. This is because the normal unidirectional crystal growth becomes preferential at these conditions. Although nanotube-like structure is attractive due to its high surface area, titanate nanotubes with free-alkali ions are usually unstable at high temperature (~500 °C) and convert into anatase particles [20, 24, 25]. To maintain the 1-D nanostructure at higher temperature (typically at 500–800 °C), the solid nanowire form is expected to be more favorable.

In this paper, pure TiO₂(B) NWs and WO₃-doped TiO₂(B) NWs (WO₃/TiO₂(B)NWs) were prepared via hydrothermal method. The effect of doping dosage on crystal structure, morphology, band gap energy, and defect concentration of the as-prepared samples were characterized and discussed in details.

2. Materials and methods

2.1. Synthesis of WO₃/TiO₂(B)NWs by hydrothermal method

In a typical preparation procedure, 1 g of TiO₂ (P25, Degussa) nanopowders mixed with 30 mL of 10 M sodium hydroxide (NaOH, 98%, Loba-chemie) and WO₃ (99.9%, Sigma-aldrich) at 0, 1, 3, and 5 mol%. The mixture was then sonicated for 1 h and transferred to 50 mL a teflon-lined autoclave container and heated at 220°C for 24 h. After cooling to room temperature, the mixture was taken out, and rinsed with 0.1 M HCl, deionized water and subsequently with ethanol, prior to drying and annealing at 400°C for 2 h.

In this research, the samples with WO₃ doping at 0, 1, 3, and 5 mol% were denoted as pure TiO₂, 1WO₃/TiO₂, 3WO₃/TiO₂, and 5WO₃/TiO₂, respectively.

2.2. Characterization of WO₃/TiO₂(B)NWs

The X-ray diffraction (XRD) patterns were characterized in terms of phase compositions and crystallite size by using an X-ray diffractometer (Phillips E'pert MPD, CuK_α). The crystallite size was determined using the Scherer equation (1) [26],

$$D = 0.9\lambda / \beta \cos\theta \quad (1)$$

where D is the crystalline size (nm), λ is the wavelength of the X-ray radiation (CuK_α=0.15406nm), β is the angle width at half maximum height, and θ is the half diffraction angle in degree of the centroid of the peak. The unit cell volume of TiO₂(B) phase was estimated from monoclinic system [20] using $\beta = 107.29^\circ$. Morphology and elemental composition of the synthesized products were examined by field emission scanning electron microscope (FE-SEM, Apreo, FEI) at acceleration voltage of 5 kV and energy-dispersive x-ray (EDX, Oxford), respectively. Band gap energy (E_g) values were obtained from UV-vis absorption spectra by UV-vis spectrophotometer (UV-2401, Shimadzu), using BaSO₄ as reference. Chemical composition was investigated by X-ray photoelectron spectrometer (XPS, AXIS ULTRA, Kratos analytical, AlK_{α1,2}).

3. Results and discussion

3.1. XRD Analysis

XRD patterns of the hydrothermal products doped with 0-5 mol% WO₃ are presented in Fig. 1. The averaged crystallite sizes were calculated and presented in Table 1. It was found that the diffraction patterns of as-prepared samples matched the monoclinic titanium dioxide (TiO₂(B) phase) in accordance with the JCPDS database 46-1238. Although WO₃ was undetected by XRD, its effect was observed. Left shift at the diffraction peak position of $2\theta = 25.32^\circ$ occurred when

WO₃ was introduced. The more left shifting of the peak position was noticed when dosing higher amounts of WO₃. The observation might be due to the differences in ionic radii between W⁶⁺ (0.60 Å) and Ti⁴⁺ (0.605 Å), there by inducing some changes in the lattice parameters [13, 27]. As shown in Table 1, the lattice parameters and unit cell volume were altered when WO₃ was incorporated. The unit cell volume decreased with the increased WO₃ dosage, suggesting that W atoms may substitute the sites of O atoms in the lattice of TiO₂(B). Furthermore, as compared to the pure TiO₂, the doped samples exhibited much smaller crystal size; 10-12 nm for the doped products and 20 nm for the pure TiO₂.

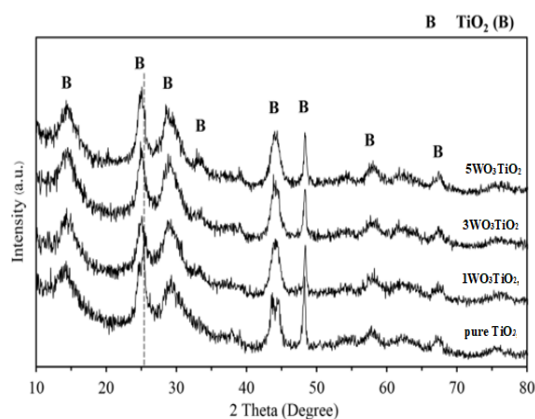


Fig. 1. XRD patterns of pure TiO₂, 1WO₃TiO₂, 3WO₃TiO₂ and 5WO₃TiO₂ calcined at 400 °C for 2 h.

Table 1. Crystallite size, Lattice parameters and unit cell volume of pure TiO₂ and WO₃/TiO₂.

Sample	Crystallite size (nm)	Lattice parameters (Å)			Cell volume (Å ³)
		a	b	c	
Pure TiO ₂	20.69	12.20	3.75	6.53	286.13
1WO ₃ TiO ₂	10.34	11.54	3.75	6.51	269.60
3WO ₃ TiO ₂	11.81	11.40	3.75	6.50	265.92
5WO ₃ TiO ₂	11.81	11.13	3.76	6.47	258.43

3.2. Morphology of as-synthesized WO₃/TiO₂

Shapes and sizes of the as-prepared WO₃/TiO₂ samples were observed by FE-SEM as illustrated in Fig. 2. Clearly, all samples exhibited wire-like shape with a diameter range of ~128–210 nm and several microns in length. As compared to the pure TiO₂, the effect of WO₃ dosages on morphology was unobvious due to the remained shapes and sizes of the doped samples at all dosages. Elemental composition of the 1 mol% WO₃/TiO₂ was demonstrated as an EDX spectrum presented in Fig. 3. The spectrum shows the presence of Ti, O, C and Na elements. The observation of Ti and O were attributed to the formation TiO₂ NWs. The presence of Na element can be ascribed to the residual elements from the precursor solution by the hydrothermal method itself. The C element was from the carbon tape used for SEM-sample preparation. W element, however, was undetected for 1 mol% WO₃ sample by EDX due to low concentration of WO₃.

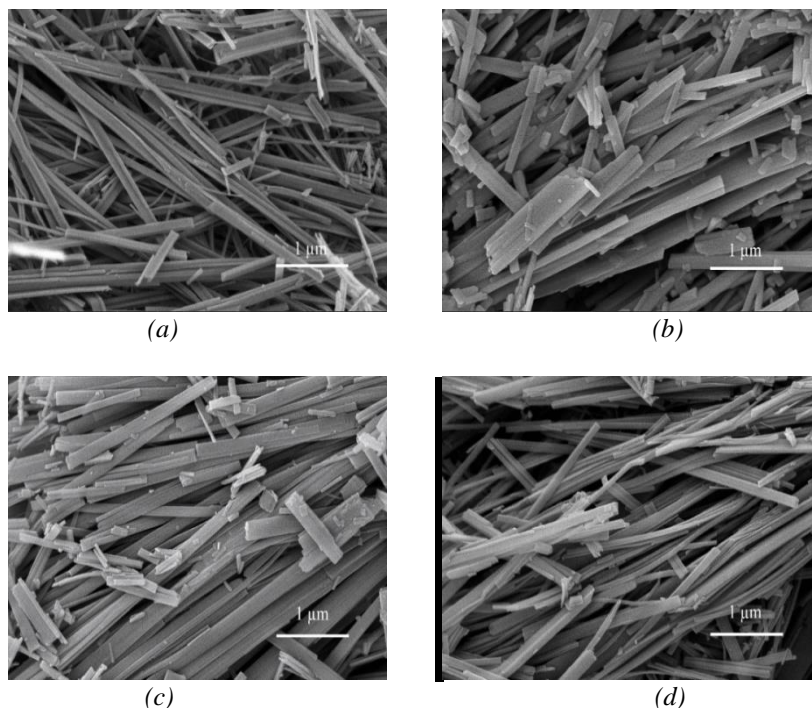


Fig. 2. FE-SEM images of (a) pure TiO_2 , (b) $1\text{WO}_3/\text{TiO}_2$, (c) $3\text{WO}_3/\text{TiO}_2$ and (d) $5\text{WO}_3/\text{TiO}_2$ NWs calcined at 400°C for 2 h.

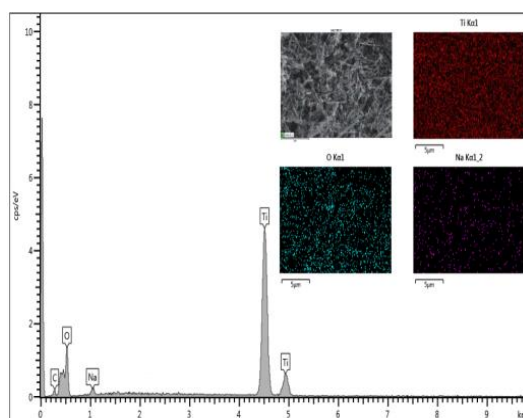


Fig. 3. EDX spectrum of $1\text{WO}_3/\text{TiO}_2$ calcined at 400°C for 2 h. (insert shows EDX mapping of Ti, O and Na elements).

3.3. XPS spectra of WO_3/TiO_2 NWs

Fig. 4 shows XPS spectra of pure TiO_2 and $1\text{WO}_3/\text{TiO}_2$ samples. The presence of O, Ti, and C elements were clearly detected from both samples, but an extra W element was found as the fourth element from the doped sample. For $1\text{WO}_3/\text{TiO}_2$ sample, atomic fractions for O, Ti, C, and W estimated by semiquantitative analysis were 53.33, 20.25, 24.76 and 1.66 at%, respectively, and the binding energies of O1s, Ti2p, C1s and W4f were 529.8, 458.8, 284.8 and 36.8 eV, respectively. It was noticed that the binding energy of Ti2p was slightly increased (see Fig.5a-b and Table 2).

As shown in Fig. 5c-d, the O1s band was modified with the introduction of the W species. For the pure TiO_2 (B) NWs, three oxygen contributions were taken into account. The peak at 529.96 eV was assigned to the oxygen bound to Ti, while the other peaks were related to the hydroxyl groups binding energy (BE) 531.3 eV and the oxygen in C-O or C=O bonds BE 532.7

eV, respectively. As shown in Fig. 5e, the determination of the exact peak positions of W4f was difficult because of the overlap with the Ti3p peak and the binding energies at 36.8 eV. However, these positions are virtually the same as those of pure WO_3 [28, 29], suggesting the oxidation state of the incorporated tungsten species is +6.

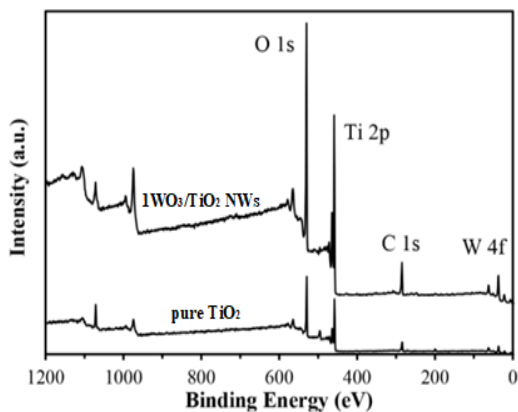


Fig. 4. XPS spectra of pure TiO_2 and $1\text{WO}_3/\text{TiO}_2$ NWs calcined at 400°C for 2 h.

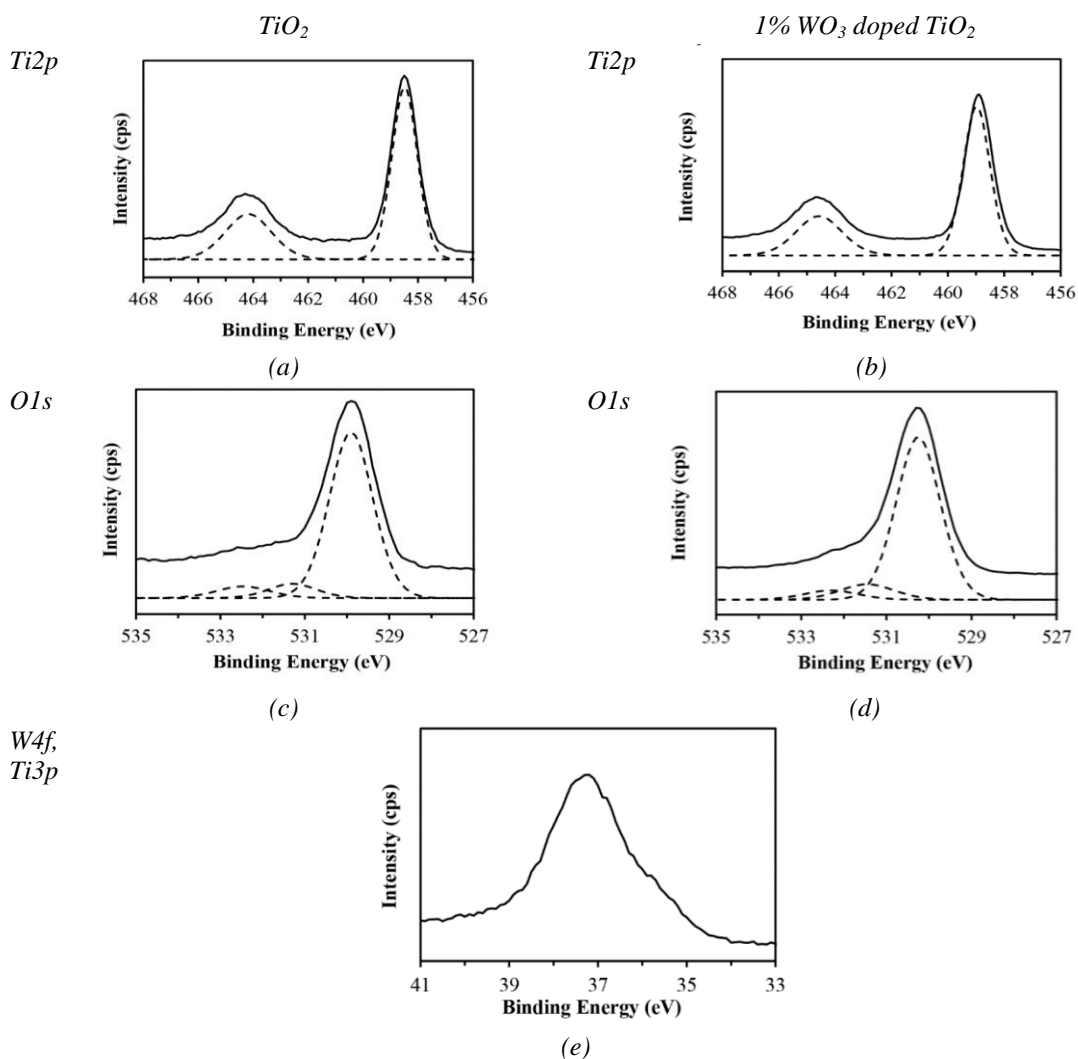


Fig. 5. XPS spectra of (a) $\text{Ti}2p$ and (c) $\text{O}1s$ of pure TiO_2 and (b) $\text{Ti}2p$, (d) $\text{O}1s$ and (e) $\text{W}4f$ of $1\text{WO}_3/\text{TiO}_2$ calcined at 400°C for 2 h.

Table 2. XPS analysis results for the pure TiO₂ and 1WO₃/TiO₂ NWs.

Peaks	Bonds	Binding energies (eV)	
		Pure TiO ₂	1WO ₃ doped TiO ₂
O1s	(Ti-O)	529.3	529.8
	(-OH)	531.2	531.6
	(C-O)	532.4	532.7
Ti2p		458.3	458.8
C1s		284.3	284.8
W4f, Ti3p		-	36.8

3.4. Energy gap measurement

The UV-vis absorption is related to the electronic transition from filled valence states to empty conduction states. Here, the absorbance of samples was measured as a function of wavelength in the range of 200-800 nm as shown in Fig. 6a. Based on the absorption spectra, the direct band-gap of all samples could be estimated from the following relationship (2) [30, 31]:

$$\alpha E = A'(E - E_g)^m \quad (2)$$

where α is the optical absorption coefficient, A' is a constant, E is the photon energy ($E=hc/\lambda$), E_g is the direct band gap energy, and $m=1/2$ for direct band gap. Generally, α can be calculated by equation:

$$\alpha=A/d' \quad (3)$$

where A is the measured absorbance and d' is the thickness of samples in a UV-vis cell (0.4 cm) and E was approximated by:

$$E=1240/\lambda \quad (4)$$

where λ is the measured wavelength in nanometers.

The extrapolation of a linear part of the curve of $(\alpha h\nu)^2$ as a function of E to $\alpha E=0$ (where $E=E_g$), as shown in Fig. 6b, is referred to as a direct band-gap of the sample. It was found that the band gap energies of the doped samples decreased with the increased WO₃ content. The decrease in band gap energy of about 0.01-0.02 eV when WO₃ was incorporated into TiO₂(B) NWs suggested that W atoms may substitute the sites of O atoms in the lattice of TiO₂ [13, 27]. Furthermore, WO₃ acted as a defect in the TiO₂ lattice which Fermi level might be located at higher level as donor band below the conduction band region of TiO₂ NWs [18, 19]. The defect concentration was estimated from the following relationship (5) [32]

$$\alpha = \alpha_0 \exp(h\nu/E_u) \quad (5)$$

where α is the absorption coefficient estimated from the measured absorbance, α_0 is a constant, E is the photon energy ($E= h\nu$), and E_u is the energy of the band tail or sometimes called Urbach energy, which an empirical parameter depends on the defect concentration and structural disorder. The defect concentration of WO₃/TiO₂ was estimated by a plot of $\ln(\alpha)$ as a function of photon energy curves and the results was shown in Fig. 6c. Reciprocal values that referred to the amount of defect concentration (E_u) were shown in Table 3. It was found that, 5 mol% WO₃ doped TiO₂ had the highest defect concentration because the WO₃ dopant acted as an impurity acceptor in TiO₂ lattice. The increase in defect concentration can improve the efficiency of the separation of electrons and holes and the absorption ability for visible light [Ref]. Moreover, defect concentration around grain boundaries strongly affects the motion of charge carriers suggesting the performance in electrical conductivity and photocatalytic activity [17, 18, 33] of the materials.

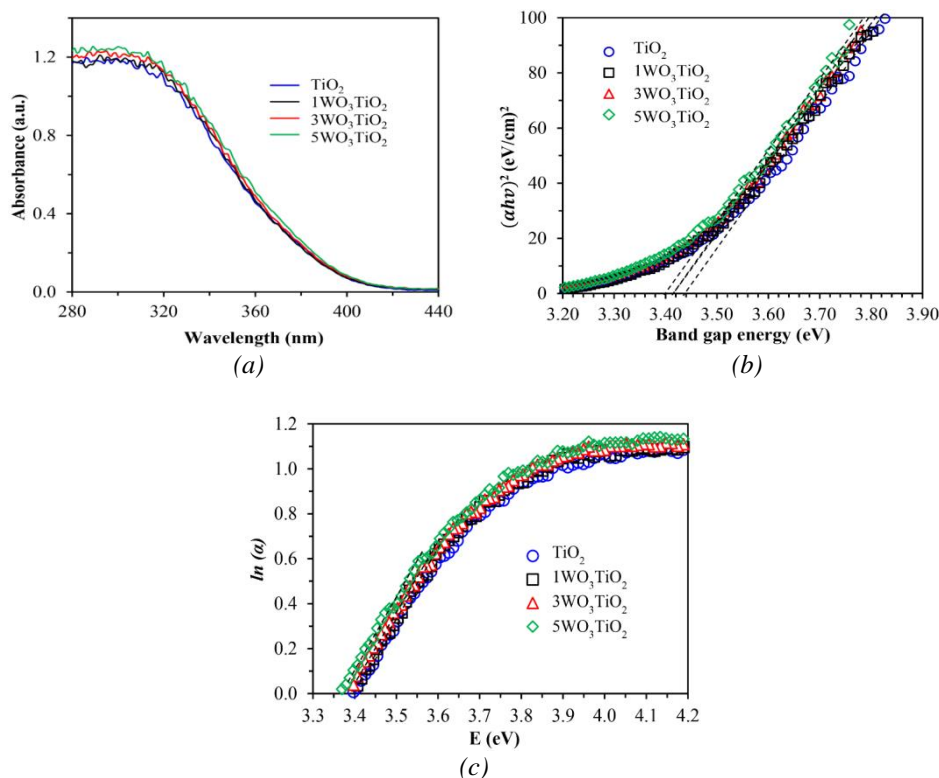


Fig. 6. (a) UV-vis spectra, (b) evolution of $(\alpha h\nu)^2$ vs. photon energy curves and (c) The plots of $\ln(\alpha)$ vs. photon energy curves for evaluating the defect concentration of pure TiO_2 and WO_3/TiO_2 NWs calcined at 400°C for 2 h.

Table 3. Band gap energy and defect concentration of pure TiO_2 and WO_3/TiO_2 NWs.

Sample	Band gap energy (eV)	Defect concentration
Pure TiO_2	3.42	0.362
$1\text{WO}_3/\text{TiO}_2$	3.41	0.348
$3\text{WO}_3/\text{TiO}_2$	3.41	0.364
$5\text{WO}_3/\text{TiO}_2$	3.40	0.376

4. Conclusion

$\text{WO}_3/\text{TiO}_2(\text{B})\text{NWs}$ were successfully prepared via hydrothermal process. Only monoclinic structure was formed at the calcination temperature of 400°C for 2 h. Doping $\text{TiO}_2(\text{B})$ NWs with WO_3 affected crystallite size, lattice parameter, unit cell volume, band gap energy, and defect concentration of the doped samples. Doping 5 mol% WO_3 into $\text{TiO}_2(\text{B})$ NWs provided the highest defect concentration, suggesting the material with high electrical conductivity and hence promising applications for ionic batteries and electrochemical sensors.

Acknowledgements

The authors would like to acknowledge Prince of Songkla University (Contract No ENG600213S) for financial support. The authors also wish to acknowledge the Center of Excellence in Materials Engineering (CEME) and the Department of Mining and Materials Engineering, the Faculty of Engineering, the Graduate School, Prince of Songkla University for facility provision.

References

- [1] A. Fujishima, K. Honda, *Nature* **238**, 37 (1972).
- [2] X. Chen, S. S. Mao, *Chemical Reviews* **107**, 2891 (2007).
- [3] S. K. Mohapatra, M. Misra, V. K. Mahajan, K. S. Raja, *Journal of Catalysis* **246**, 362 (2007).
- [4] R. Marchand, L. Brohan, M. Tournoux, *Materials Research Bulletin* **15**, 1129 (1980).
- [5] M. Tournoux, R. Marchand, L. Brohan, *Progress in Solid State Chemistry* **17**, 33 (1986).
- [6] T. P. Feist, S. J. Mocarski, P. K. Davies, A. J. Jacobson, J. T. Lewandowski, *Solid State Ionics* **28-30**, 1338 (1988).
- [7] T. P. Feist, P. K. Davies, *Journal of Solid State Chemistry* **101**, 275 (1992).
- [8] J.-H. Lee, M.-H. Hon, Y.-W. Chung, C. Leu, *Applied Physics* **102**, 545 (2011).
- [9] Q. Hu, C. Wu, L. Cao, B. Chi, J. Pu, L. Jian, *Journal of Power Sources* **226**, 8 (2013).
- [10] D. Maheswari, P. Venkatachalam, *Measurement* **60**, 146 (2015).
- [11] T. A. Kandiel, A. Y. Ahmed, D. Bahnemann, *Journal of Molecular Catalysis A: Chemical* **425**, 55 (2016).
- [12] Z. Chen, J. Zhao, X. Yang, Q. Ye, K. Huang, C. Hou et al., *Industrial and Engineering Chemistry Research* **55**, 80 (2016).
- [13] B. Pal, B. L. Vijayan, S. G. Krishnan, M. Harilal, W. J. Basirun, A. Lowe et al., *Journal of Alloys and Compounds* **740**, 703 (2018).
- [14] W. Zhan, H. Ni, R. Chen, Z. Wang, Y. Li, J. Li, *Thin Solid Films* **548**, 299 (2013).
- [15] X. Luo, F. Liu, X. Li, H. Gao, G. Liu, *Materials Science in Semiconductor Processing* **16**, 1613 (2013).
- [16] F. Shi, J.-X. Liu, X. Huang, L. Yu, S.-H. Liu, X. Feng et al., *Advanced Powder Technology*, **26**, 1435 (2015).
- [17] L. Jing, B. Xin, F. Yuan, L. Xue, B. Wang, H. Fu, *The Journal of Physical Chemistry B* **110**, 17860 (2006).
- [18] H.-X. Tong, Q.-Y. Chen, Z.-L. Yin, H.-P. Hu, D.-X. Wu, Y.-H. Yang, *Transactions of Nonferrous Metals Society of China* **19**, 1483 (2009).
- [19] Q. Zhang, X.-J. Li, F.-B. Li, J. Chang, *Acta Physico-Chimica Sinica* **20**, 507 (2004).
- [20] R. Yoshida, Y. Suzuki, S. Yoshikawa, *Journal of solid state Chemistry* **178**, 2179 (2005).
- [21] A. R. Armstrong, G. Armstrong, J. Canales, P. G. Bruce, *Angewandte Chemie - International Edition* **43**, 2286 (2004).
- [22] G. H. Du, Q. Chen, P. D. Han, Y. Yu, L. M. Peng, *Physical Review B* **67**, 035323 (2003).
- [23] Y. Suzuki, S. Pavasupree, S. Yoshikawa, R. Kawahata, *Journal of Materials Research* **20**, 1063 (2005).
- [24] Y. Suzuki, S. Yoshikawa, *Journal of Materials Research* **19**, 982 (2004).
- [25] R. Yoshida, Y. Suzuki, S. Yoshikawa, *Materials Chemistry and Physics* **91**, 409 (2005).
- [26] H.-L. Qin, G.-B. Gu, S. Liu, *Comptes Rendus Chimie* **11**, 95 (2008).
- [27] P. S. Archana, A. Gupta, M. M. Yusoff, R. Jose, *Physical Chemistry Chemical Physics* **16**, 7448 (2014).
- [28] J. H. Pan, W. I. Lee, *Chemistry of Materials* **18**, 847 (2006).
- [29] Z. DohLeviL-MitroviL, S. StojadinoviL, L. Lozzi, S. AškrabiL, M. RosiL, N. TomiL et al., *Materials Research Bulletin* **83**, 217 (2016).
- [30] S. Suwanboon, P. Amornpitoksuk, A. Sukolrat, *Ceramics International* **37**, 1359 (2011).
- [31] P. Jittiarporn, L. Sikong, K. Kooptarnond, W. Taweepreda, *Ceramics International* **40**, 13487 (2014).
- [32] A. Hassanien, A. A. Akl, *Superlattices and Microstructures* **89**, 153 (2016).
- [33] H. Wittmer, S. Holten, H. Kliem, H. D. Breuer, *Physica status solidi A* **181**, 461 (2000).